Limit-cycles prevention via multiple $\mathcal{H}_\infty$ constraints with an application to anti-windup design

Jean-Marc Biannic *

* *ONERA, The French Aerospace Lab.*
System Control and Flight Dynamics Department
BP 74025, F–31055 Toulouse Cedex, France

Abstract: Rate and magnitude control limitations are often responsible for the apparition of undesired limit-cycles in the resulting nonlinear closed-loop system. Based on the well-known describing function approach, it is shown in this paper that such limit cycles can be avoided as soon as H_∞ constraints are simultaneously satisfied by appropriately chosen linear interconnections. This result is then used to design anti-windup compensators.

Keywords: Limit cycles, anti-windup, saturations, H_∞ control.

1. INTRODUCTION

As observed by Impram and Munro [2004], the stability analysis of nonlinear control systems can often be treated as a problem of investigating the existence of sustained oscillations known as limit-cycles. Although the detection of such oscillatory behavior cannot be regarded as a rigorous stability test for nonlinear systems, the knowledge of their existence and characteristics (magnitude and frequency) is often crucial to predict wether the plant will become unstable or not. A variety of techniques have then been developed in the past decades to detect and avoid limit-cycles among which describing function (DF) methods (Gelb and Van der Velde [1968], Mees and Bergen [1975]) are still very popular today thanks to their close connections with linear frequency-domain techniques (Ackermann and Bunte [1997]). Interestingly, these techniques offer possibilities for systematic control systems design in the presence of input saturations (Hippe and Wurmthaler [1999]) which are always present in practice. This is especially true in flight control systems (Fielding and Flux [2003]). Inspired by such results, the central contribution of this paper is based on these classical frequency-domain conditions to check the existence of limit-cycles in magnitude and rate limited control systems. The main result consists of a new characterization of the above conditions via multiple $\mathcal{H}_\infty$ constraints from which a new anti-windup design approach (Kothare et al. [1994], Hippe [2010], Zaccarian and Teel [2011], Tarbouriech [2011]) can be derived.

The paper is organized as follows. Backgrounds on describing functions in the context of magnitude and rate saturations are briefly recalled first. Then, the main technical results devoted to limit-cycle prevention are developed in section 3. A straightforward application of these results to anti-windup is then proposed in section 4. Next, a short illustration is detailed in section 5. Finally, some concluding remarks end the paper.

⋆ When this work was carried out, the author was also affiliated to LAAS-CNRS, Toulouse.

2. DESCRIBING FUNCTIONS AND CRITICAL LOCI FOR MAGNITUDE AND RATE LIMITATIONS

Consider a class of nonlinear systems as depicted in Figure 1. It consists of feedback loops of a possibly unstable linear transfer function $F(s)$ and a dynamic nonlinearity Ψ resulting from the cascade of magnitude and rate saturations. The limiting operator Ψ which in

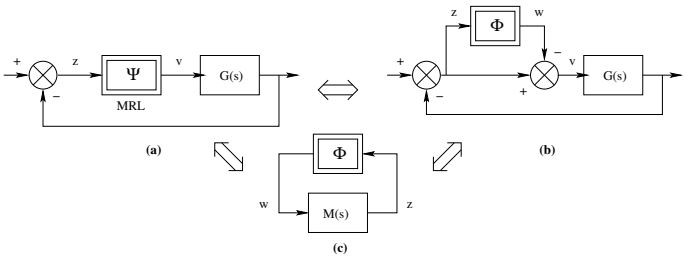

Fig. 1. Magnitude and rate limited feedback systems: original and standard forms.

practice is usually placed at the output of the control system to prevent saturations in the physical actuators is visualized by the diagram of Figure 2. By a standard loop transformation, this operator can be conveniently replaced by a new one denoted $\Phi = I - \Psi$ which, in nominal conditions (without saturations), verifies $\Phi \equiv 0$.

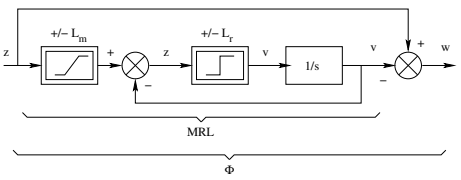

Fig. 2. Block-diagram of a Magnitude and Rate Limiting (MRL) operator.

Remark 1. From this transformation, it results that the linear interconnection $M(s) = (I + G(s))^{-1}G(s)$ in Figure

1.c coincides with the nominal closed-loop plant and is then always stable.

In the specific context of sinusoidal-input describing function (SIDF) analysis, the input signal $z(t)$ is assumed to be $z(t) = x \sin \omega t$. Then, the output $v(t) = \Psi(x \sin \omega t)$ is a periodic signal and the describing function gain is defined as the fundamental of the Fourier series of $v(t)$ divided by the input amplitude x. Denoted $N_\Psi^{(1)}$, the resulting complex-valued gain generally depends on both the amplitude x and the frequency ω. Its general expression for the k^{th} harmonic reads:

$$N_\Psi^{(k)}(x,\omega) = \frac{j\omega}{\pi x} \int_0^{\frac{2\pi}{\omega}} \Psi(x \sin \omega t) e^{-jk\omega t} dt \qquad (1)$$

When analytical expressions are not available, the above expressions is easily computed numerically for fixed values of x and ω (see Schwartz and Gran [2001]). In the case of magnitude and rate saturations, analytical expressions can be obtained, but a total six different configurations needs to be considered according to the shape of the output signal $v(t)$ over a period:

- (NL): Non-Limited signal. Neither the magnitude nor the rate limitation is active in this case,
- (ML): Magnitude-Limited signal . Only the magnitude saturation is active here,
- (RL1): Rate-Limited signal, type 1. The output signal is triangular and then remains rate-bounded during the whole period,
- (RL2): Rate-Limited signal, type 2. The output signal is partially rate-bounded,
- (MRL1): Magnitude and Rate-Limited signal, type 1. The signal is either magnitude or rate limited during the cycle,
- (MRL2): Magnitude and Rate-Limited signal, type 2. This is the most complex situation where the output signal can be either magnitude-limited or rate-limited or non constrained at all during the cycle.

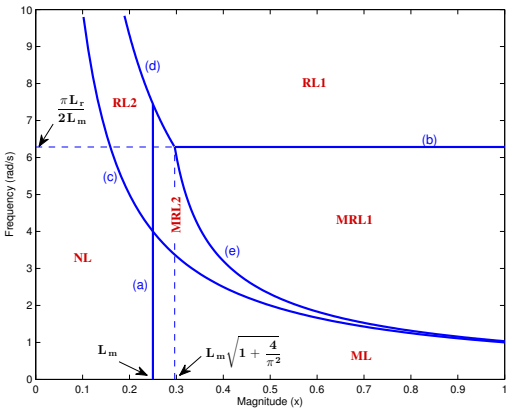

Fig. 3. Visualization of the six possible operating modes of the mixed Magnitude & Rate Limiting operator for a sinusoidal input signal.

These six regions are visualized on Figure 3 in the plane (x, ω). The boundaries are defined by two straight lines $((a), (b))$ and three hyperbolic curves $((c), (d), (e))$:

$$\begin{array}{ll} (\mathbf{a}):\ x = L_m & (\mathbf{d}):\ \omega x = L_r \left(1 + \frac{\pi^2}{4}\right)^{\frac{1}{2}} \\ (\mathbf{b}):\ w = \frac{\pi L_r}{2L_m} & \\ (\mathbf{c}):\ \omega x = L_r & (\mathbf{e}):\ \omega x = L_r \left(1 - \frac{L_m^2}{x^2}\right)^{-\frac{1}{2}} \end{array} \qquad (2)$$

For two standard cases, when the signal is either severely magnitude limited (ML) or fully rate limited (RL1), the expressions of the SIDF gains remain rather simple. In the first case, the gain is real. It coincides with that of a pure relay nonlinearity and only depends on x:

$$N_\Psi^{(1)}(x,\omega) = N_\Psi(x) = \frac{4L_m}{\pi x} \qquad (3)$$

In the second case, a complex-valued gain is obtained (the rate saturation induces a phase delay):

$$N_\Psi^{(1)}(x,\omega) = \frac{4L_r}{\pi \omega x} e^{-j \arccos \frac{\pi L_r}{2\omega x}} \qquad (4)$$

Interestingly, in this last situation, the gain only depends on the product ωx. Next, observing that for the above considered time-invariant nonlinearity Ψ, one obtains:

$$N_\Psi^{(2)}(x,\omega) = 0\,,\ N_\Psi^{(3)}(x,\omega) \approx \frac{1}{3} N_\Psi^{(1)}(x,\omega) \qquad (5)$$

the standard assumptions of describing function analysis are verified as soon as the linear model $G(s)$ in Figure 1 acts as a low-pass filter. In such conditions, the existence of limit-cycle oscillations (with amplitude x_c and frequency ω_c) in the nonlinear closed-loop plant of Figure 1.a can be investigated through the resolution of the harmonic balance equation (see for example the comprehensive book of Gelb and Van der Velde [1968] for further details):

$$1 + G(j\omega_c) N_\Psi^{(1)}(z_c, \omega_c) = 0 \qquad (6)$$

The resolution of the above equation is usually performed graphically in the Nyquist or Nichols plane by looking for intersections between the Nyquist plot of $G(s)$ and the critical loci of the nonlinearity $-1/N_\Psi^{(1)}(x,\omega)$.

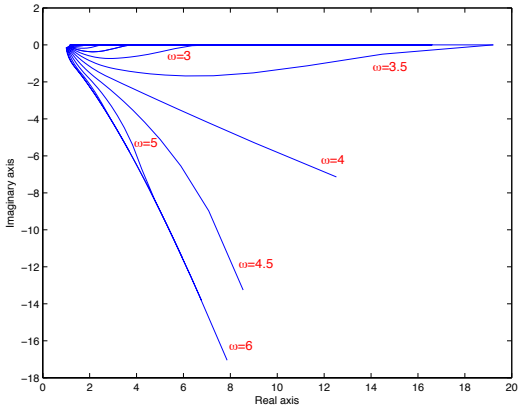

Fig. 4. Visualization of the critical loci $1/N_\Phi^{(1)}(x,\omega)$ in the Nyquist plane (with $L_r = 1$ and $L_m = 0.25$).

Instead of considering the standard equation (6) to investigate the existence of limit cycles, it is proposed in this paper to base the analysis on Figure 1.c, which yields:

$$M(j\omega_c) = 1/N_\Phi^{(1)}(x_c, \omega_c) \qquad (7)$$

with

$$N_{\Phi}^{(1)}(x_c, \omega_c) = 1 - N_{\Psi}^{(1)}(x_c, \omega_c) \tag{8}$$

The critical loci of interest for solving (7) graphically will now take the form visualized by Figure 4.

3. AVOIDING LIMIT-CYCLES

Let us assume that the linear part $G(s)$ or equivalently $M(s)$ can be modified by the designer so as to minimize the risk of limit cycle in the nonlinear closed-loop plant. This assumption is not restrictive since either $G(s)$ or $M(s)$ generally includes a tunable controller. From the above discussion on the existence of limit cycles, it can be claimed that if the following conditions hold:

$$\forall \omega \geq 0, \forall x \geq 0, \quad M(j\omega) \neq 1/N_{\Phi}^{(1)}(x, \omega) \tag{9}$$

then no limit cycle will appear in the systems of Figure 1. From Figure 4, it appears that the most simple way to enforce the above conditions consists of constraining the Nyquist plot of $M(s)$ to remain strictly inside the unit disk, which is visualized on Figure 5 by vertical hatching. Since $M(s)$ coincides with the nominal closed-loop plant

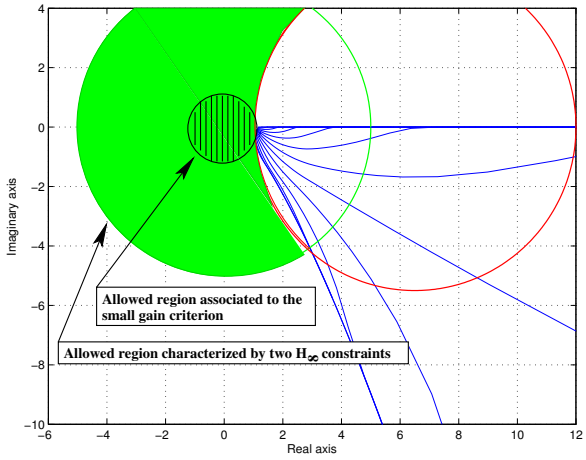

Fig. 5. Examples of $\mathcal{H}_\infty$-constrained regions in the Nyquist plane such that conditions (9) for no limit-cycle to exist are verified.

and is then strictly stable, the above condition may be reformulated as a single $\mathcal{H}_\infty$ constraint.

$$\forall \omega \geq 0, |M(j\omega)| < 1 \Leftrightarrow \|M(s)\|_\infty < 1 \tag{10}$$

Well known as the small gain criterion, this constraint is extremely conservative in the context of limit-cycle prevention in the presence of magnitude and rate limitations. It indeed ensures stability for any (possibly time-varying) nonlinear bounded operator Ψ such that $\|\Psi(z)\| \leq \|z\|$.

As illustrated by Figure 5, much less conservative regions (shaded in green) can be defined in the Nyquist plane to avoid intersections between the Nyquist locus of $M(s)$ and the critical loci. Among various possibilities, a simple strategy consists in relaxing condition (10) as follows:

$$\|M(s)\|_\infty < c_1 \tag{11}$$

with $c_1 > 1$, and to introduce additional constraints keeping the Nyquist locus outside a region which contains the intersections of the critical loci with the disk centered at the origin with radius c_1 as defined in (11). For the ease of characterization, a natural choice for such a region is also a disk, in which case the additional constraint reads:

$$\forall \omega \geq 0, |M(j\omega) - \alpha| > \rho \tag{12}$$

where the center $\alpha > c_1$ and radius $\rho \geq \alpha - 1$ need to be appropriately chosen in order to minimize conservatism. Using the following lemma, the above condition can be rewritten as an $\mathcal{H}_\infty$ constraint (with $c_2 = \alpha/\rho$):

$$\|(I - \alpha^{-1}M(s))^{-1}\|_\infty < c_2 \tag{13}$$

Lemma 2. Given a positive scalar α and a stable LTI model $M(s)$, such that $\|M(s)\|_\infty < \alpha$, then the linear feedback interconnection $T(s) = (I - \alpha^{-1}M(s))^{-1}$ is well-posed and for any positive real c, the $\mathcal{H}_\infty$ constraint:

$$\|T(s)\|_\infty = \|(I - \alpha^{-1}M(s))^{-1}\|_\infty < c \tag{14}$$

guarantees that the Nyquist plot of $M(s)$ remains **outside** the disk $\mathcal{D}(\alpha, \alpha/c)$ with center α and radius $\rho = \alpha/c$. □

Sketch of proof: Since $\|M(s)\|_\infty < \alpha$, well-posedness and stability of the interconnection $T(s)$ result from the small-gain theorem. Next, the $\mathcal{H}_\infty$ constraint (14) clearly implies, $\forall \omega \geq 0, |1-\alpha^{-1}M(j\omega)|^{-1} < c \Leftrightarrow |M(j\omega)-\alpha| > c$. ■

In many practical situations, limit cycles cannot be avoided. This typically appears when the open-loop plant $G(s)$ is unstable. In this case the Nyquist locus will generally intersect the critical loci near 1 and it is no longer possible to minimize the bound c_2 in (13) until the radius ρ verifies $\rho \geq \alpha - 1$ to exclude 1. In such cases, the impact of limit-cycles on closed-loop stability is often minimized when either their frequency or amplitude is large.

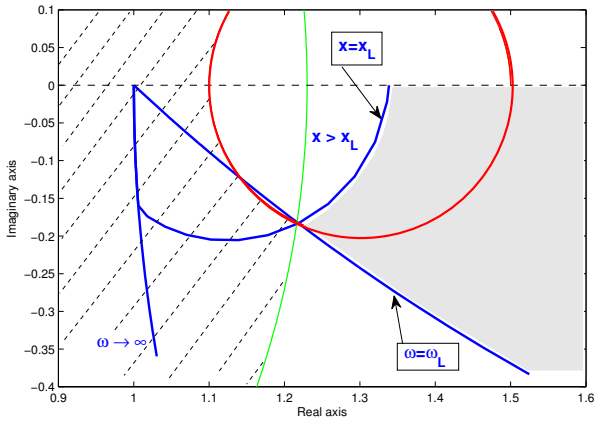

Fig. 6. Example of $\mathcal{H}_\infty$ constrained regions such that possible limit cycles have large amplitude ($x_c > x_L$) or high frequency ($\omega_c > \omega_L$).

Exploiting more precisely the geometry of the critical loci, it is rather easy to define a region $\mathcal{R}$ in the Nyquist plane such that: if $\forall \omega \geq 0, M(j\omega) \notin \mathcal{R}$ then any possible limit

cycle will either be such that $x_c > x_L$ or $\omega_c > \omega_L$. This region, visualized in gray on Figure 6 can be avoided when the two $\mathcal{H}_\infty$ constraints (11) and (13) are simultaneously satisfied for a new choice of c_1, c_2 and α. These two constraints are visualized by oblique hachures. Here again, this criterion based on mutliple $\mathcal{H}_\infty$ constraints is much less conservative than what would have been obtained by a single constraint derived from the small gain theorem.

4. APPLICATION TO ANTI-WINDUP DESIGN

4.1 Notation and problem formulation

Following the notation introduced in Ferreres and Biannic [2007] and Biannic and Tarbouriech [2009], let us now consider the anti-windup control problem depicted in Figure 7. Given a possibly unstable LTI model $G(s)$ and a nominal controller $K(s)$, the objective is to compute an anti-windup gain $J(s)$ which will modify the control law as soon as magnitude or rate limitations are activated ($w \neq 0$). Let us redraw the standard interconnection of Figure 7.a as shown on Figure 7.b and define the partition $L(s) = [L_1(s)\ L_2(s)]$. The new transfer $M(s) = \mathcal{T}_{w\to z}(s)$ "seen" by the nonlinear operator Φ now reads:

$$M(s) = L_1(s) + L_2(s)J(s) \tag{15}$$

and clearly depends on $J(s)$ which can be designed so as to shape the Nyquist plot of $M(s)$ in such a way that potential limit-cycles are either eliminated or modified.

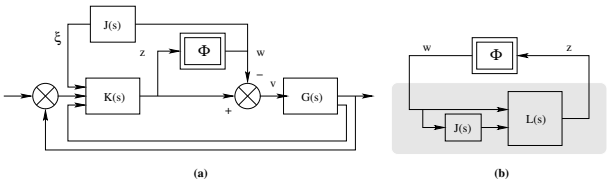

Fig. 7. Anti-windup general structure

4.2 Resolution via multi-objective $\mathcal{H}_\infty$ design

Let us now combine the results of section 3 with the above formulation. It immediately follows that an anti-windup compensator can be obtained as the solution of the following multi-objective $\mathcal{H}_\infty$ optimization problem:

$$\hat{J}(s) = arg \min_{J(s)} \max \left(\mu \|T_1(s)\|_\infty, \|T_2(s)\|_\infty\right) \tag{16}$$

with (for given design parameters $\alpha > 0$ and $\mu \geq 0$):

$$\begin{aligned} T_1(s) &= (L_1(s) + L_2(s)J(s)) \\ T_2(s) &= \left(I - \alpha^{-1}(L_1(s) + L_2(s)J(s))\right)^{-1} \end{aligned} \tag{17}$$

The above optimization problem is generally nonconvex but can be solved quite efficiently today thanks to recent advances in nonsmooth optimization techniques. These have initially permitted to solve fixed-order $\mathcal{H}_\infty$ control problems (Burke et al. [2006] and Apkarian and Noll [2006a]) with one $\mathcal{H}_\infty$ constraint. Next, the case of several constraints corresponding to the problem (16) to be solved here has also been considered (Gumussoy et al. [2009], Apkarian and Noll [2006b]) and numerical tools for use with MATLAB© (see Gahinet and Apkarian [2011] or Overton et al. [2006]) are now available.

5. A SHORT ILLUSTRATION

Let us now illustrate and further discuss the proposed anti-windup design technique on two simple examples.

5.1 A marginally stable open-loop plant

Consider the following second-order open loop model with input u and output θ:

$$G(s) = \frac{1}{s(s+0.1)} \tag{18}$$

Next define a stabilizing PID controller for this plant:

$$u(t) = \int_0^t (\theta_c(\tau) - \theta(\tau))d\tau - 2.5\theta(t) - 2.4\dot{\theta}(t) \tag{19}$$

The nominal closed-loop (without saturations) reads:

$$\mathcal{T}_{\theta_c\to\theta}(s) = \frac{1}{(s+1)(s^2+1.5s+1)} \tag{20}$$

Let us introduce magnitude ($L_m = 0.25$) and rate ($L_r = 1$) limitations on the control signal u and let us apply a step input with amplitude $\theta_c = 2.114$. In such conditions, limit-cycle oscillations clearly appear in the system as shown on Figure 8 where the initial and bounded $u_L(t) = \Psi(u(t))$ control signals are visualized (with dashed and solid lines respectively). The dotted line corresponds to a sinusoidal approximation of $u \approx x_c \sin(\omega_c t)$.

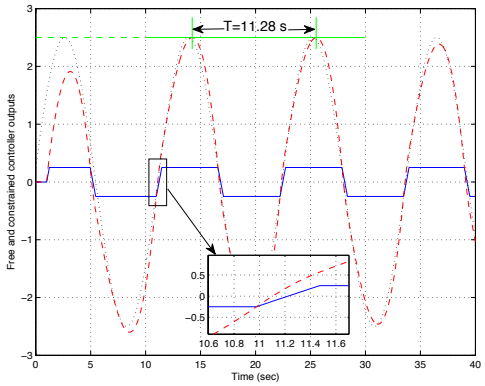

Fig. 8. Visualization of an unstable limit-cycle

This limit-cycle is confirmed by describing function analysis. As is visible on Figure 9, intersections exist between the Nyquist plot of $M(s)$ and the critical loci $1/N_\Phi$.

As proposed in Section 4 an anti-windup compensator is now designed to eliminate the above limit-cycle by "shaping" the Nyquist plot. To this purpose, following standard schemes, the anti-windup action is placed on the integrator so that the control law is modified as follows:

$$u(t) = \int_0^t (\theta_c(\tau) - \theta(\tau) + \xi(\tau))d\tau - 2.5\theta(t) - 2.4\dot{\theta}(t) \tag{21}$$

where the signal $\xi(t)$, following the notation of Figure 7, denotes the output of the anti-windup compensator $J(s)$.

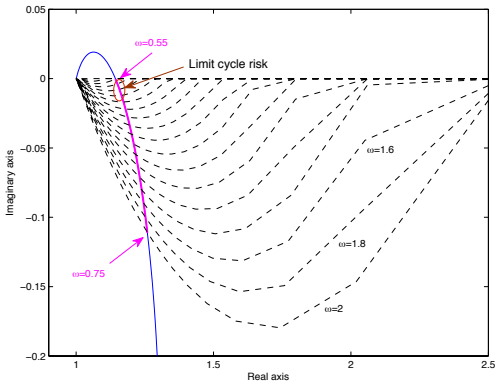

Fig. 9. Limit-cycle detection in the Nyquist plane

From this structure, the linear interconnection $L(s)$ is readily obtained as follow:

$$L(s) = \frac{[1 + 2.5s + 2.4s^2 \quad -s(s + 0.1)]}{(1 + s)(1 + 1.5s + s^2)} \tag{22}$$

and the multi-objective $\mathcal{H}_\infty$ design problem (16) can thus be implemented in a fairly straightforward way with the help of either the "HIFOO 3.5" MATLAB© package (Overton et al. [2006]) or the "HINFSTRUCT" routine (Gahinet and Apkarian [2011]) which is available with the Robust Control Toolbox. The design parameters are initially fixed to $\alpha = 1.5$ and $\mu = 1$ and a static controller $J(s) = J$ is optimized. The best $\mathcal{H}_\infty$ norm for this choice is around 3.6 and coincides with $\|T_2(s)\|_\infty$. The design parameter μ is then increased until $\mu = 2.9$. For this value, both constraints are equal: $\mu\|T_1(s)\|_\infty = \|T_2(s)\|_\infty = 3.6$ and one obtains: $\hat{J} = 1.53$. As expected, with this tuning,

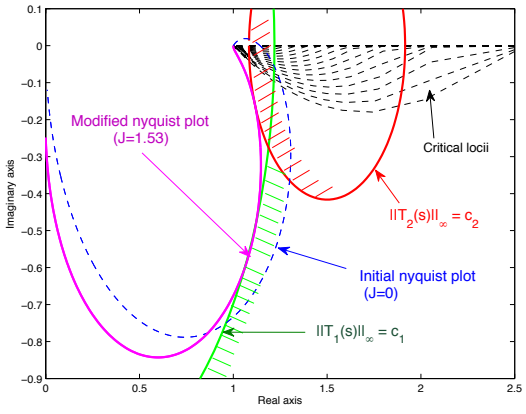

Fig. 10. Anti-windup effect: limit-cycle elimination

the modified transfer "seen" by the nonlinear operator Φ does no longer intersect the critical loci so that the risk of limit-cycles has been cancelled. This transfer, visualized by the magenta solid line in Figure 10 is constrained inside the green disk ($\|T_1(s)\|_\infty \leq c_1$) and outside the red one ($\|T_2(s)\|_\infty \leq c_2$). The absence of limit cycle is confirmed by the nonlinear simulations visualized on Figure 11. For the same constant input $\theta_c = 2.114$ as before, the oscillations have now disappeared. Note that for this case, arbitrarily high step inputs can be applied to the system which has been globally stabilized by the anti-windup compensator.

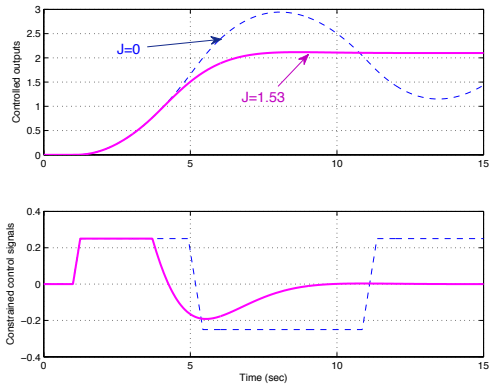

Fig. 11. Comparisons of nonlinear closed-loop step responses with or without anti-windup.

5.2 A strictly unstable open-loop plant

Let us modify the open-loop model as follows:

$$G(s) = \frac{1}{s(s - 0.1)} \tag{23}$$

and consider the same PID controller as before. Without saturations, the closed-loop behavior is very close to the previous case. In the presence of magnitude and rate saturations a limit-cycle appears with slightly increased amplitude and frequency (see Figure 12). Now, the largest step input is $\theta_c = 1.7$. Let us then design a new anti-

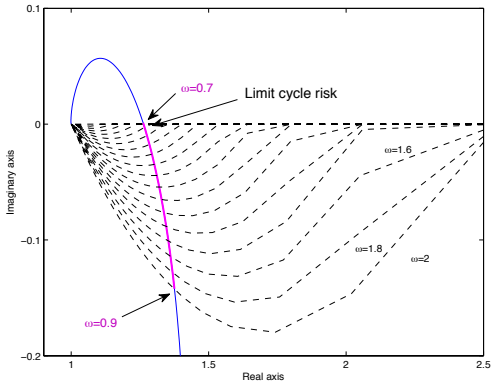

Fig. 12. Limit-cycle detection in the Nyquist plane with open-loop unstable plant

windup compensator so that stability and performance are still preserved for large step inputs. The same structure as before is used. The multi-objective $\mathcal{H}_\infty$ optimization problem is first solved for $\alpha = 1.5$ and $\mu = 1$. The last parameter is then increased to $\mu = 1.4$. For this value both constraints have the same norm: $\mu\|T_1(s)\|_\infty = \|T_2(s)\|_\infty = 4.7$ and one obtains $\hat{J} = 0.98$. As expected, the transfer is modified so that its intersections with the critical loci are now closer to the critical point 1 and thus correspond to higher magnitude (see Figure 13). The risk of limit-cycle is then not completely eliminated. This is not surprising since the nonlinear closed-loop plant

cannot be globally stabilized here. However, by increasing the amplitude of the limit cycle, it is expected that the stability domain is enlarged. Although this fact cannot be proved in the general case, it is often verified in practice and this is the case here. Observing the plots of Figure 13, even though the anti-windup device has not completely removed the risk of limit-cycle in the closed-loop system, the step responses remain close to nominal for $\theta_c = 1.7$.

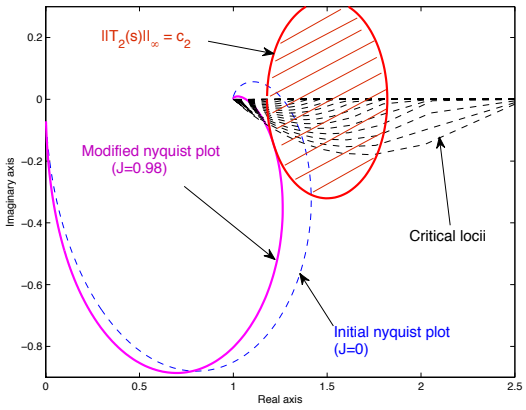

Fig. 13. Anti-windup effect: limit-cycle migration

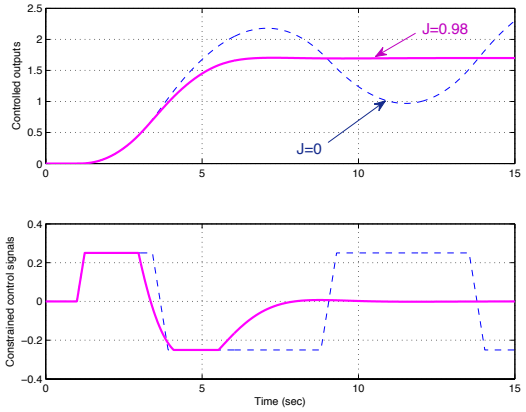

Fig. 14. Comparisons of nonlinear closed-loop step responses with or without anti-windup.

6. CONCLUSIONS

Based on the well-known describing function approach, it has been shown in this paper that limit cycles, for a specific class of nonlinear control systems, can be avoided as soon as H_∞ constraints are simultaneously satisfied by appropriately chosen linear interconnections. This result has then been used in the context of anti-windup design. The proposed methodology is successfully evaluated on a simple example which has been chosen for its tutorial value. Interestingly, the proposed approach is still applicable for very high order systems. Future works will be devoted to extensions of the anti-windup design approach to systems involving multiple and possibly more general nonlinearities. A specific attention will also be devoted to the tuning aspects so that the design procedure can be automatized and made available to non expert users.

REFERENCES

J. Ackermann and T. Bunte. Robust prevention of limit cycles for robustly decoupled car steering dynamics. *Kybernetika*, 35(1):105–116, 1997.

P. Apkarian and D. Noll. Nonsmooth $\mathcal{H}_\infty$ synthesis. *IEEE Trans. on Aut. Contr.*, 51(1):71–86, 2006a.

P. Apkarian and D. Noll. Nonsmooth optimization for multidisk $\mathcal{H}_\infty$ synthesis. *European Journal of Control*, 12(3):229–244, 2006b.

J-M. Biannic and S. Tarbouriech. Optimization and implementation of dynamic anti-windup compensators in aircraft control systems with multiple saturations. *Control Engineering Practice*, 17(6):703–713, June 2009.

J.V. Burke, D. Henrion, A.S. Lewis, and M.L. Overton. Stabilization via nonsmooth optimization. *IEEE Trans. on Aut. Contr.*, 51(11):1760–1769, Nov. 2006.

G. Ferreres and J-M. Biannic. Convex design of a robust anti-windup controller for an LFT model. *IEEE Trans. on Aut. Contr.*, 52(11):2173–2177, Nov. 2007.

C. Fielding and P.K. Flux. Non-linearities in flight control systems. *Aeronautical journal*, 107(1077):673–686, 2003.

P. Gahinet and P. Apkarian. Structured H_∞ synthesis in MATLAB. In *Proceedings of the IFAC World Congress*, pages 1435–1440, Milan, Italy, Sept. 2011.

A. Gelb and W.E. Van der Velde. *Multiple-input describing functions and nonlinear system design.* McGraw-Hill electronic sciences series. McGraw-Hill, 1968.

S. Gumussoy, M. Millstone D. Henrion, and M.L. Overton. Multiobjective Robust Control with HIFOO 2.0. In *Proceedings of the IFAC Symposium on Robust Control Design*, Haifa, 2009.

P. Hippe. *Windup in Control: Its Effects and Their Prevention.* Advances in Indus. Contr. Springer, 2010.

P. Hippe and C. Wurmthaler. Systematic closed-loop design in the presence of input saturations. *Automatica*, 35(4):689–695, April 1999.

S.T. Impram and N. Munro. Limit cycle analysis of single-loop feedback systems with multiple nonlinearities and parameter uncertainties. *European Journal of Control*, 10(2):119–130, February 2004.

M. Kothare, P. Campo, M. Morari, and C. Nett. A unified framework for the study of anti-windup designs. *Automatica*, 30(12):1869–1883, December 1994.

A. Mees and A.R. Bergen. Describing functions revisited. *IEEE Trans. on Aut. Contr.*, 20(4):473–478, Aug 1975.

O. Overton, M. Millstone, D. Henrion, S. Gumussoy, G. Deaconu, and D. Arzelier. HIFOO 3.5. A MATLAB package for fixed order controller design. 2006. Available at: http:// www.cs.nyu.edu/overton/software/hifoo/.

C. Schwartz and R. Gran. Describing function analysis using MATLAB and SIMULINK. *IEEE Control Systems Magazine*, 21(4):19–26, August 2001.

S. Tarbouriech. *Stability and stabilization of linear systems with saturating actuators.* Springer London, 2011.

L. Zaccarian and A.R. Teel. *Modern anti-windup synthesis.* Princeton University Press, 2011.